Analysis of a numerical benchmark for columnar solidification of binary alloys

Hervé Combeau, Michel Bellet, Yves Fautrelle, Dominique Gobin, Eric Arquis, Olga Budenkova, Bernard Dussoubs, Yves Duterrail, Arvind Kumar, Charles-André Gandin, et al.

Analysis of a Numerical Benchmark for Columnar Solidification of Binary Alloys

H. Combeau[1*], M. Bellet[2], Y. Fautrelle[3], D. Gobin[4], E. Arquis[5], O. Budenkova[3], B. Dussoubs[1], Y. Du Terrail[3], A. Kumar[1], Ch.-A. Gandin[2], B. Goyeau[6], S. Mosbah[1], T. Quatravaux[1], M. Rady[5], M. Založnik [1]

1 Institut Jean Lamour, CNRS – Université de Lorraine, Département SI2M, Ecole des Mines de Nancy, Parc de Saurupt CS14234, F-54042 Nancy cedex, France
2 MINES ParisTech & CNRS, CEMEF UMR 7635, 06904 Sophia Antipolis cedex, France
3 EPM-SIMAP - CNRS – INPG – Université Joseph Fourier, 38402 St Martin d'Hères cedex, France
4 FAST - CNRS – Université Pierre et Marie Curie, 91405 Orsay cedex, France
5 I2M- Dpt TREFLE - CNRS – Université de Bordeaux – Arts et Métiers ParisTech – ENSCBP, 33607 Pessac Cedex, France
6 EM2C - CNRS – Ecole Centrale Paris, 92295 Châtenay-Malabry, France

E-mail: herve.combeau@ijl.nancy-universite.fr

Abstract. During the solidification of metal alloys, chemical heterogeneities at the scale of the product develop. It is referred to as "macrosegregation". Numerical simulation tools exist in the industry. However, their predictive capabilities are not validated and are still limited. A 2D numerical benchmark is presented, based on the solidification of metallic Pb-Sn alloys. Concerning the numerical benchmark, a "minimal" common model of solidification is assumed, including columnar growth without undercooling, fixed solid, isotropic permeability of the mushy region, local thermodynamic equilibrium, lever-rule assumption for the local average composition. We focus our attention on the numerical method used to solve the average conservation equations: Finite Volume, Finite Element, Velocity-Pressure coupling treatment, scheme for convective terms, etc. At this stage of the work, we cannot exhibit a reference solution. However we draw some conclusions on the effects of the grid dependency, in particular on the location and sizes of the segregate channels. The development of both thermally and solutal driven convections in the first stage of the process (cf. low Prandtl and high Lewis numbers) and the relative independency of the convective scheme are also discussed. This presentation also have the goal to call other contributors to join this benchmark [1] in order to enrich the exercise and to reach a reference solution for this important problem in metallurgy.

1. Introduction

In the field of production of metal products, the solidification step is responsible of the formation of defects such as heterogeneities of composition (macrosegregation) and structure extending at the scale of the product [1]. The reduction of these defects is an important issue for industry because it damages the quality of the final properties of products. Numerical simulation is a valuable tool for progress in

this direction. However, computer codes are not yet fully predictive. Several reasons are related to that which can be attributed on one side to the modeling aspect and on the other side to numerical aspects.
The macrosegregation is caused by relative movements of solid and liquid phases such as: natural convection, flow induced by shrinkage for the liquid phase; grain motion, solid skeleton deformation for the solid phase [1]. Due to the complexity of the involved phenomena which take place over several characteristic length scales of space and time, there description by models is till now incomplete, even if only one of these phenomena is considered. The transport equations accounting for the different length scales are derived by an averaging technique [2-4] or the mixture theory [5]. By these two methods we can use a single set of equations in the whole domain (fully liquid, mushy zone and fully solid). At the beginning of the development of these models, simple assumptions concerning the transport phenomena at the microscopic scale were adopted, like the lever rule for the microsegregation. As the microsegregation is at the origin of the macrosegregation, several works have been dedicated to microsegregation models applicable for macrosegregation predictions [6-11]. Notably, macrosegregation has already been predicted with microsegregation models that were coupled with thermodynamic databases [10, 11, 13, 17]. The improvement of the description of the microstructure was also an important center of interest. By introducing the concept of the grain envelops to define a boundary between the grains and the liquid outside of the grains [7], it was possible to predict the evolution of the grain morphology. The most refined models predict the columnar to equiaxed transition [11], the grain size, the grain morphology and the macrosegregation induced by the motion of the grains and the interdendritic liquid [15]. The prediction of channel segregates was also the topic of many studies. Most of them were concerned with freckles, corresponding to a situation where the thermal gradient is oriented in the same direction as the gravity [1, 17]. Only few of them were related to other situations of solidification. Some studies were devoted to the case where the thermal gradient is perpendicular to the gravity. It was shown that the mesh size is the main parameter for channels prediction [14]. Refinement of the mesh size conduced to a change in the curvature of the channels and induced a preferential path of the flow inside the channels. Investigations on 3D effects started only recently [12, 16, 28]. Two different shapes of channel have been predicted, a first one with a tubular section whereas the second one is lamellar. Until now, the few experimental results available in the literature reported tubular channels [16]. More experimental investigations need to be done to confirm the existence of lamellar channels.
Concerning numerical simulation, difficulties are inherent to the values of the thermophysical properties in case of metals. Thermal or solutal natural convection are difficult to simulate with a good accuracy for liquid metals because of the low value of the Prandtl number (~ 0.01) on one hand and the great value of the Lewis number (~ 104). Nonlinearities in the equations like the permeability term in the momentum equation need also to be carefully accounted for in the discretization, as well as the strong coupling between the transport phenomena which necessitate developing specific algorithms [20,22].
In 2007, we decided to launch the SMACS project centered on the prediction of macrosegregation. This project involves five French laboratories: CEMEF, IJL, EM2C, EPM-SIMAP, and TREFLE. The aims of this project are one hand to compare the predictions of computer codes on base cases in natural convection and solidification (numerical benchmark); on the other hand, to qualify the quality of the prediction of the models by comparisons with experiments carried out at EPM-SIMAP [24]. For the numerical benchmark, the model has been fixed for all the partners and chosen as simple as possible with regard to the description of solidification, whereas for the second part the choice of the model was open.
This communication aims to present some of the results obtained in the benchmark part of the SMACS project. These results concern one of the two reference cases defined in the solidification part of the benchamrk and are relative to the formation of macrosegregation during the solidification of a Pb-18 wt% Sn alloy in a 2D cartesian domain.

2. Presentation of one of the two benchmark test cases in solidification

This test case consists to simulate the solidification of an alloy Pb-18 wt% Sn in a rectangular cavity of 0.1 m wide and 0.06 m high (see Figure 1).

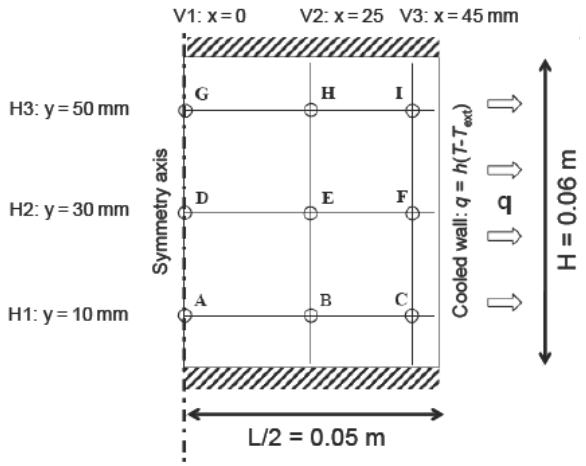

Figure 1. Description of the solidification problem (boundary conditions and locations of the horizontal and vertical lines as well as the locations of the points used for the outputs).

The top and bottom walls are assumed to be adiabatic, while the two vertical walls are cooled: a Fourier condition, the same for both sides is imposed. For the flow, a non-slip condition is imposed on all the boundaries of the domain. Due to the symmetry of geometry and boundary conditions and assuming again the symmetry of the solution, only half the field was considered. At the initial time, the alloy is assumed at rest (no velocity) and its temperature equal to the liquidus temperature corresponding to its nominal composition (285.5 ° C). The geometry of the domain, the boundary conditions and the location of the outputs are shown in Figure 1.

The model describing the solidification has been set; each partner has taken care to solve the same system of equations. The equations expressing the conservation of: energy, global mass, momentum and mass of solute were derived from the method of averaging volume. By taking the order listed above these equations are written as:

$$\rho \frac{\partial \langle h \rangle}{\partial t} + \rho c_p \nabla T \cdot \mathbf{V} - \nabla \cdot (k \nabla T) = 0 \tag{1}$$

$$\nabla \cdot \mathbf{V} = 0 \tag{2}$$

$$\rho \frac{\partial \mathbf{V}}{\partial t} + \frac{\rho}{g_l} (\nabla \mathbf{V}) \mathbf{V} = \nabla \cdot (\mu_l \nabla \mathbf{V}) - g_l \nabla p - \frac{\mu_l g_l}{\mathrm{K}} \mathbf{V} + g_l \rho (1 - \beta_T (T - T_0) - \beta_c (C_l - C_0)) \mathbf{g} \tag{3}$$

$$\frac{\partial \langle C \rangle}{\partial t} + \nabla C_l \cdot \mathbf{V} = 0 \tag{4}$$

The definition of the variables is given in the nomenclature at the end of this document. The chosen microsegregation model corresponds to the complete thermodynamic equilibrium between liquid and solid phases (lever rule):

$$\langle C \rangle = g_l C_l + g_s C_s = \left(g_l + (1 - g_l) k_0 \right) \cdot C_l \tag{5}$$

$$T = T_m + m_l C_l \tag{6}$$

Full details of the case with all the thermo-physical data and definition of outputs can be downloaded on a dedicated website [25] and in ref [18].

Five computer codes have been used to simulate this test case. Four computer codes are based on the finite volume formulation (FVM) (FLUENT 6.2 (EPM-SIMAP), THETIS (TREFLE/EM2C) [2], SOLID (IJL) [20] and OpenFOAM (IJL)) and one code is based on the finite element method with unstructured triangular meshes (FEM) (R2SOL (CEMEF) [21]) (see Table 1). For FLUENT, THETIS and OpenFOAM solvers the energy conservation equation (1) is solved with the temperature as the main unknown. For R2SOL and SOLID solvers, equation (1) is solved with the mass average enthalpy as the main unknown [20]. For these two codes, the solute mass conservation equation (4) is solved with the average composition as the main unknown, following the scheme proposed by Voller [22]. In the case of EPM-SIMAP, this equation is separated in two parts, one for the liquid phase and one for the solid phase. For the discretization in space of the convective terms, a second order scheme was used in the case of TREFFLE (RST) and EPM-SIMAP (second order upwind), IJL in case of SOLID used a 1st order upwind scheme and in case of OpenFOAM used a first order upwind or a QUICK scheme, whereas CEMEF used an SUPG stabilization scheme.

Table 1. Key features of the computer codes mesh size and time step used for the results presented in this paper

Group	**Software**	**Mesh (size, average mesh size (m))**	**Time step (s)**
IJL	SOLID F.V. (upwind)	192x232 (2.6 x 10^{-4})	5 x 10^{-3}
CEMEF	R2SOL F.E. (SUPG)	46502 nodes (2.5 x 10^{-4})	5 x 10^{-3}
EPM-SIMAP	FLUENT F.V. (second order upwind)	200x240 (2,5 x 10^{-4})	5 x 10^{-3}
TREFLE	THETIS F.V. (TVD)	268x324 (1,9 x 10^{-4})	1 x 10^{-3}
IJL	OpenFOAM F.V. (upwind or QUICK)	200x240 (2,5 x 10^{-4})	5 x 10^{-3}

The meshes and time steps values used for the results presented in this paper are reported in Table 1. A sensitivity study to the mesh and time step has been carried out by each partner whose results are presented in section 4.

3. Description of the progress of the solidification

The results obtained by EPM-SIMAP are presented in this section in order to describe the evolution of solidification in the domain. The total time of solidification is about 600 seconds. From the temperature, liquid fraction and velocity fields at time 120 seconds reported in Figure 2, one can see that the isotherms are almost vertical in the region where the liquid fraction is less than 0.8 whereas there is a thermal stratification in the central part where the liquid fraction is larger. The circulation of the liquid in the domain is counterclockwise. The progressive enrichment in tin of the interdendritic liquid during solidification which decreases its density is responsible of this counterclockwise flow. This effect is dominant over the thermal effect, which explains the direction of rotation of the fluid obtained. In areas of low liquid fraction, we note the presence of channels inside which the liquid fraction is locally higher. These channels have started to form in region of high liquid fraction, early after the beginning of the solidification, after 20 seconds two channels are clearly visible. Their formation is linked to the direction of the interdendritic liquid flow with regard to the thermal gradient. A positive component of the velocity of the interdendritic liquid in the direction of the thermal gradient will induce locally a delay to the solidification which can later become a channel. One can notice that the remelting of the solid skeleton is not necessary. These channels, due to their increased

permeability, are a preferential path for the liquid flow. The temperature field as can be seen in Figure 2(a) is not strongly affected by the presence of the channels.

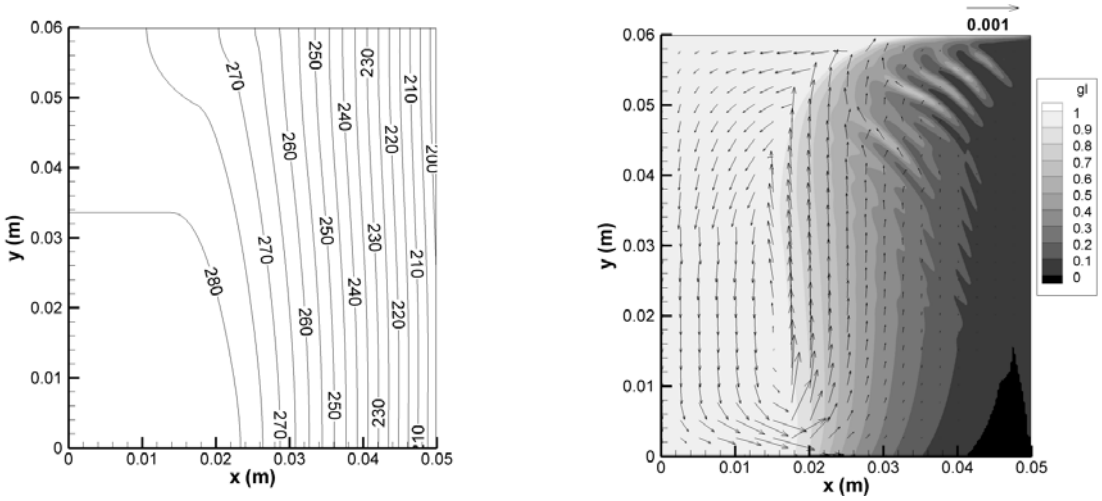

(a) (b)

Figure 2. (a) temperature field, (b) velocity field (vectors, the scale is indicated by the arrow at the top right in m s^{-1}) and liquid fraction field (grey levels) at time 120 s.

The map of the average composition in tin after the end of solidification obtained by EPM-SIMAP is shown in Figure 3(a). The upper left corner of the half cavity which is the last to solidify is positively segregated, while the bottom right region where the interdendritic liquid circulates in the reverse direction of the thermal gradient is negatively segregated. A positive segregation has also developed inside the channels associated with a negative segregation at their periphery.

4. Comparison and analysis of the results obtained by all the partners

Maps of the average concentration field at the end of solidification (t=600 s) obtained by the six codes are presented in Figure 3. The macrosegregation is in accordance with the description in the previous section and the six simulations are in qualitative agreement on the general segregation map. The principal differences are the position and the number of channel segregates. It is interesting to notice the differences between the two simulations using both OpenFOAM but with a different scheme for the discretization of the convective terms. With the upwind scheme, the channels start to form at the height of 0.04 m whereas with the QUICK scheme they start at the height of 0.045 m. More channels form in case of the upwind scheme: at the height H3 (see Figure 1 for its location), six channels are visible while only four are visible in case of the QUICK scheme. As the only difference between these two results is the discretization scheme of the convective terms, this demonstrates its strong influence on channels prediction. We can distinguish two groups of results, which coincide with the order of the convection schemes that were used. We can observe that the results from EPM-SIMAP, TREFLE and OpenFOAM QUICK, all using a second order scheme, are closer with regard to the channels. They predict the same number of channels and the height at which they formed. The same remarks can be done for the IJL and OpenFOAM upwind results. The result coming from CEMEF, the only FEM software participating to this benchmark exercise, cannot be sorted in the two previous classes. The channels start closer to the left vertical wall, and at a lower height than in the other contributions. These similarities between different contributions are re-discussed more quantitatively in a next part of this section.

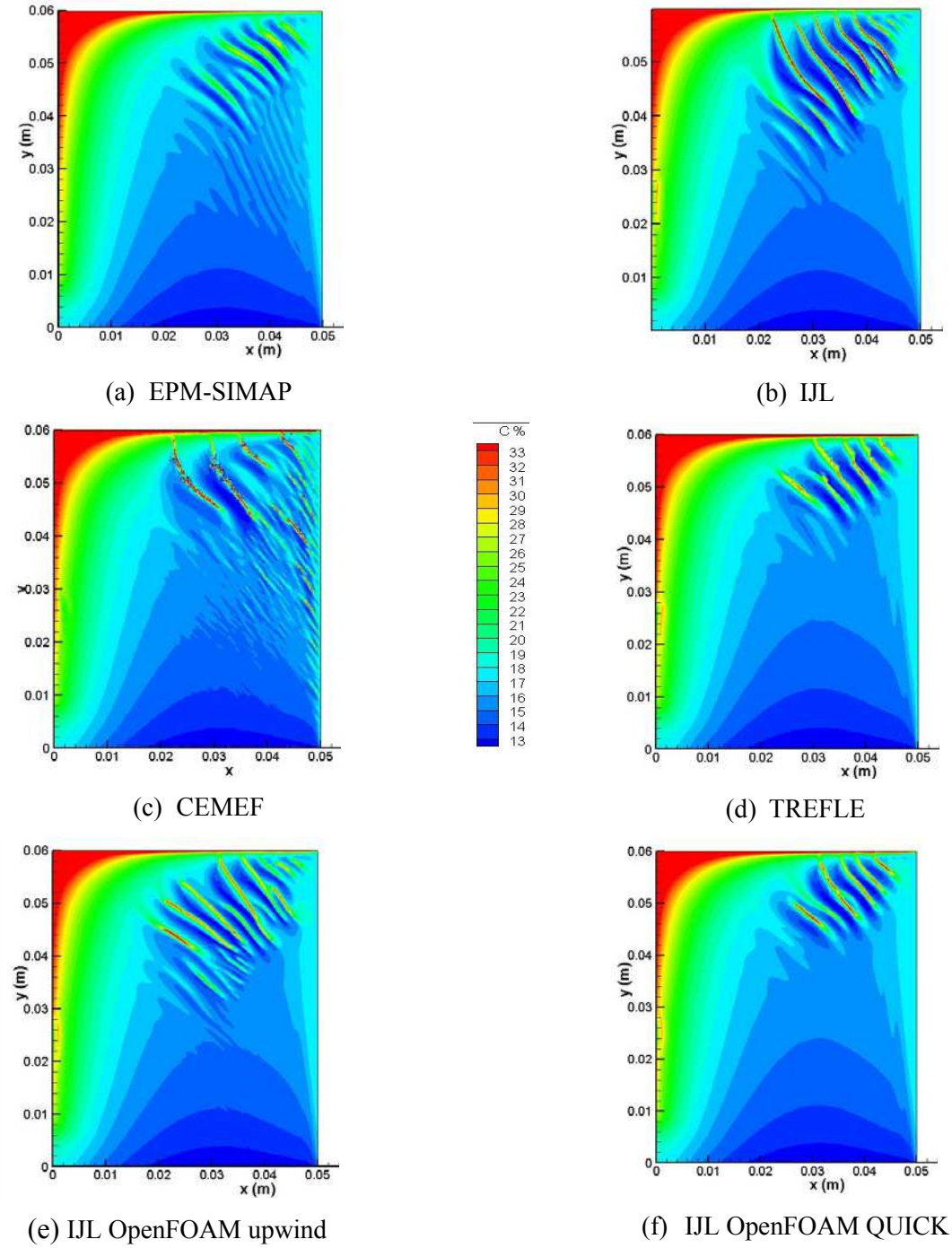

Figure 3. At the end of solidification: map of average mass concentration in Sn (wt. pct.) obtained by the different contributors. The color scale is similar for the six contributions.

In Figure 4, the horizontal profiles at height H1 and H2 (see location in Figure 1) of the final average composition in tin for all the simulations are presented. In term of macrosegregation, i.e. variations at the scale of the width of the domain, the results are similar. However, significant differences are visible in the region where the channels are located (from 0.02m to 0.05m in Figure 4(b). In this region, for all the simulations, variations of composition with stronger amplitude than for the

macrosegregation can be observed. These variations correspond to the channels formed during the solidification. However, in the zoom of Figure 4(b), it can be seen that the location and the amplitude of these variations differ in function of the simulation. Notably, in the case of OpenFOAM, the results differ between a discretization of the convective terms using a first upwind scheme and a QUICK scheme, everything else being similar in the numerical scheme. It was expected that for a relatively fine mesh like those used for the results presented in this paper, such sensitivity would have been smaller. Thus, even in the case of finer meshes, these results confirm those of reference [20] in which a first comparison exercise was conducted between two computer codes for a similar situation: macrosegregation results were similar, the main differences were also observed at the level of segregated channels.

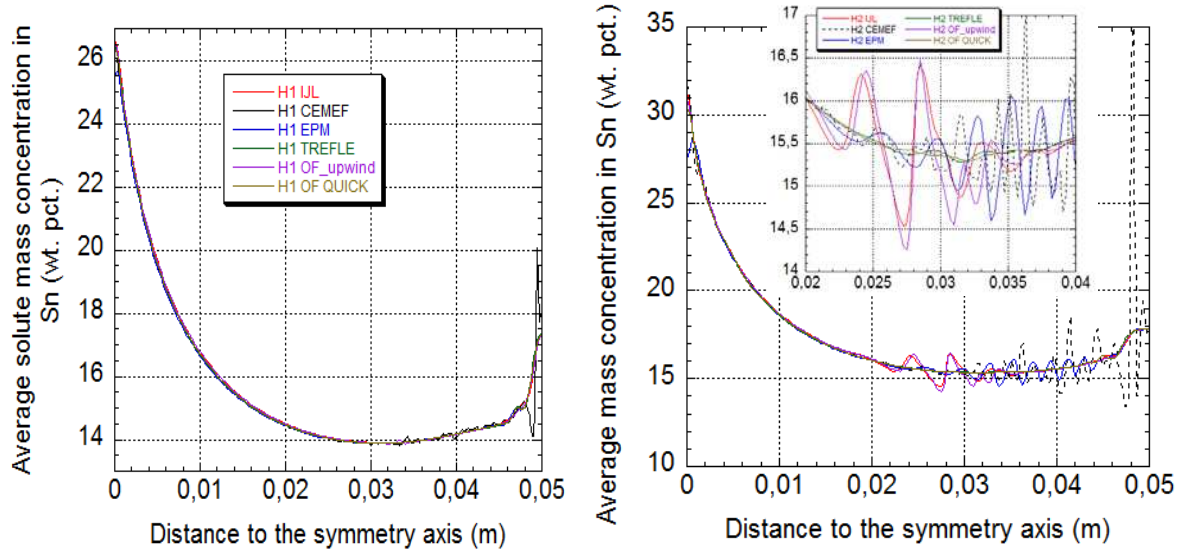

(a) (b)

Figure 4. At the end of solidification: Average mass concentration in Sn (wt. pct.): (a) along the horizontal line H1, (b) along the horizontal line H2.

In the upper part of the domain, as can be seen in Figure 3, the segregation in the channels is more severe. The horizontal profiles of concentration in Sn along the line H3 are plotted in Figure 5 for the six contributions. The height H3 is located 0.01 below the top of the cavity. As can be seen in Figure 3 this height corresponds to the mid-height of the channels. At this height, the variation of concentration across a channel is much stronger than at height H2. At the height H2, the maximum of the variation of the average concentration in Sn across a channel was of the order of 2 wt. pct, whereas this maximum is now of the order of 20 wt. pct.. The concentration varies by this magnitude on a distance of the order of 2 mm. The size of the Representative Elementary Volume (REV) used for the derivation of the volume averaged equations can be estimated by the microstructure size used to calculate the permeability. This is the only microscopic characteristic length introduced in the input data. For this benchmark case, its value is 185 µm. Thus, the average concentration in Sn varies in the order of 1.5 wt. pct over a REV located in the region of the channels, whereas this variation was only 0.15 wt. pct. at the height H2. If we look at the variation of the average concentration in Sn at the scale of the width of the domain, it is of the order of 20 wt. pct. in Sn along 0.05 m. This corresponds to a variation of concentration equal to 0.07 across a REV. To be valid, the volume averaging technique assumes that there is a separation of scales between a microscopic scale and a macroscopic scale. This implies that there is an intermediate scale corresponding to the size of the REV. At this intermediate scale, the variation of a quantity averaged in a volume of the size of the REV has to be negligible with regard to the variation at the macroscopic scale. This condition is not satisfied in the channel region,

where we get a variation of 1.5 wt. pct. in Sn across a REV, which is much greater than the variation at the macroscopic scale estimated to 0.07 wt. pct. in Sn at the scale of the REV. Therefore, the assumption of scale separation is not valid any more in a channel. This can be a reason why the results differ between the different contributions for the prediction of channels.

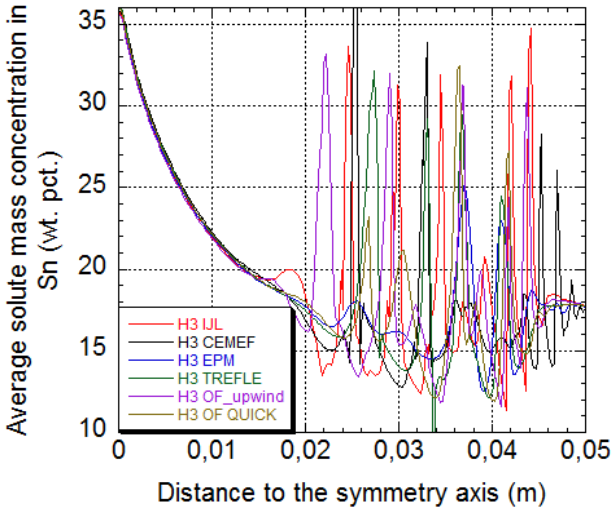

Figure 5. At the end of solidification: average mass concentration in Sn (wt. pct.) along the horizontal line H3.

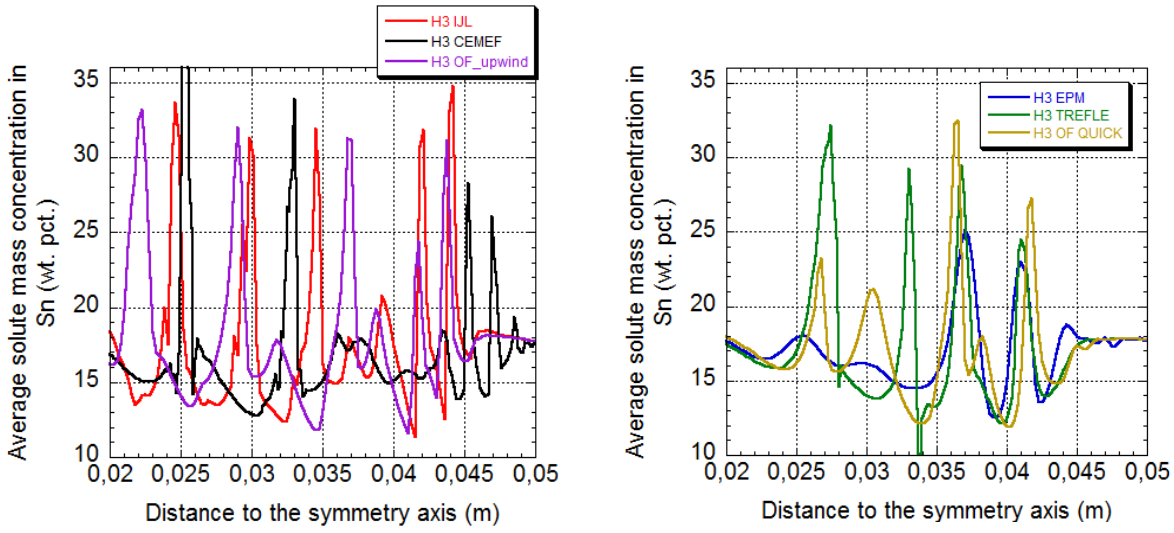

(a) (b)

Figure 6. Zoom of the average mass concentration in Sn (wt. pct.) profiles along the horizontal line H3 at the end of solidification: (a) for IJL, CEMEF, OpenFOAM_upwind contributions, (b) for EPM, TREFLE, OpenFOAM_Quick contributions.

In Figure 6, the profiles of average concentration in Sn at the height H3 are zoomed in the region of the channels. The results are plotted on two graphs: in Figure 6.a, the results of the two finite volume codes using a first order scheme for the convective term (IJL and OpenFOAM upwind) and the finite element model (CEMEF) are plotted whereas in Figure 6.b the results of the three finite volume codes

using a second order scheme for the convective terms (EPM-SIMAP, TREFLE and OpenFOAM QUICK). We have distinguished these two classes of solutions because they present similarities in terms of the amplitude of the variation of the average concentration in Sn across the channels and in terms of distance between two channels. As the global solute mass balance (equation (4)) is a purely convective equation, it is not surprising to find a high sensitivity of the order of accuracy of the interpolation scheme for the interpolation of the convective terms. It is well known [27] that a first order scheme like the upwind scheme will induce more numerical diffusion than a higher order scheme. However, even if we find similarities between the solutions produced by the same order of accuracy in space of the scheme, the results are not superimposed. For the results obtained with a finite element method (CEMEF), one can see from Figures 3 and 4.b that the channels start to form closer to the vertical right side of the domain than in the case of the other contributions.

A mesh and time step sensibility study was conducted by each contributor. While all details of these studies cannot be presented here, the most important observations are summarized. The mesh convergence observed with respect to the maximum and minimum values of the solute concentration after completed solidification is shown in Figure 7. The five codes based on the finite volume method show very similar sensibilities of the maximum value of the average concentration at the end of the solidification to the mesh density. In all cases, the order of convergence is smaller than one. For the finite element code, the maximum value seems to evolve more rapidly and is higher than for the other contributions. For all the contribution the maximum value is located in the upper left corner of the half domain which does not correspond to a channel. The sensibility of the minimum values to the mesh size is dependent of the contributor. First is has to be mentioned that the location of the minimum value is found close to the channels for all the contributors excepted for EPM-SIMAP for whose it is located in the negatively segregated region in the bottom of the cavity. As the channels are very sensitive to the mesh size and to the code, it explains why the minimum varies with the contributions.

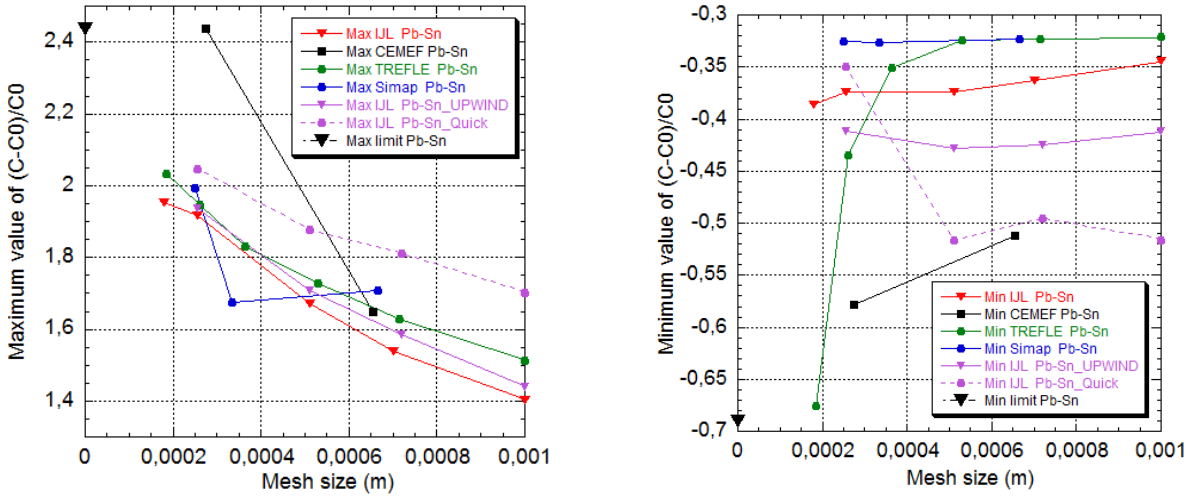

(a) (b)

Figure 7. Mesh convergence of the final relative segregation$(C-C_0)/C_0$: (a) the maximum of the field at the end of solidification, (b) the minimum of the field at the end of solidification.

The velocities of the liquid are an important element of comparison of the solutions. In Figure 8, the horizontal profiles along the horizontal line H2 of the liquid fraction and of the modulus of the intrinsic velocity of the liquid defined as: $\left\|V_l^l\right\| = \frac{\|V\|}{g_l}$ are presented at time 120 seconds. The shapes of the curves are similar for the six simulations. Similarly, the temperature profiles not included in this

communication are superimposed. The strongest differences are observed in the channels corresponding to the local fluctuations of the liquid fraction in Figure 8(a). Similarly, for points located 0.02 m farther from the symmetry axis, differences in the modulus of the intrinsic velocity of the liquid phase are correlated with the fluctuations of the liquid fraction. Differences are also visible in the region of high liquid fraction, typically for a liquid fraction greater than 0.95.

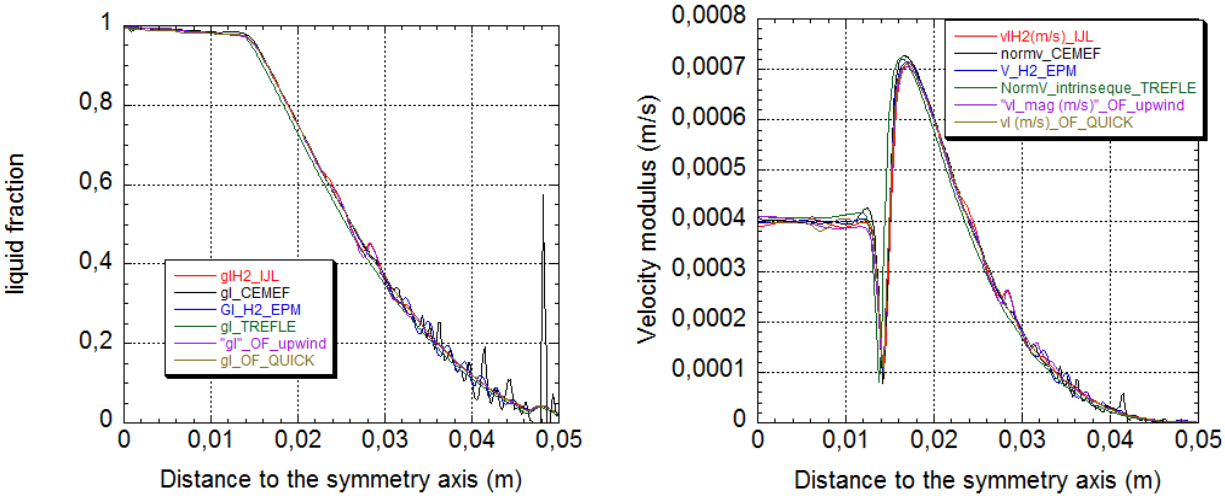

(a) (b)

Figure 8. Horizontal profiles along the line H2 (see Figure 1) at time 120 seconds, (a) liquid fraction, (b) modulus of the intrinsic velocity of the liquid phase.

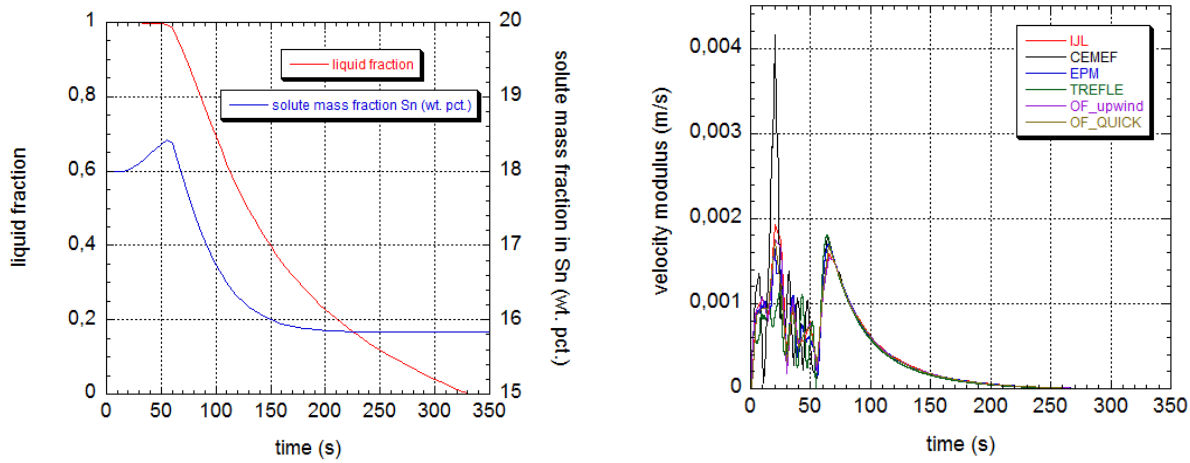

(a) (b)

Figure 9. Time evolutions at point E (see Figure 1 for its location) of (a) the solute mass fraction and liquid fraction; (b) the modulus of the intrinsic velocity of the liquid phase.

The time evolutions of the liquid fraction and of the average concentration in point E, shown in Figure 9(a), show that the macrosegregation continues to evolve even up to small liquid fractions (approximately until the liquid fraction becomes lower than 0.3). In Figure 9(b) we show the evolution of the velocity modulus in point E with time. All solutions predict overall the same evolution, after

t=70s, the velocity decreases monotonically. Some notable differences in the beginning, until t=70s are visible. This initial interval corresponds to the period when liquid fractions were high. These observations suggest an explanation for the reason why the macrosegregations are similar and the channels different. As for this case, the macrosegregations develop principally at liquid fraction lower than 0.9 below which the flow is similar for all the contributions, the prediction of the macrosegregation gives similar results for all the contributions. The flow for these liquid fractions is then dominated by the three last terms of equation (3) and the convective term in this equation is negligible. So the results are less sensitive to the discretization scheme. At the reverse the channels form at high liquid fraction for which the inertia term in equation (3) stays important. Then the results are sensitive to the discretization scheme.

5. Conclusion

This communication presents the results of the comparison between different numerical procedures in the solution of an identical 'minimal' solidification model. We can conclude that even though the qualitative image of the different solutions is the same, notable differences exist in the evolutions and local behaviors. For the final segregation map in average mass concentration in Sn, the main differences are located in the channels and in their vicinity. The number of channels and the intensity of segregation inside the channels vary from one contribution to another. Even with fine meshes, it has not been possible to find a unique solution, mesh independent and similar for all the contributions. These differences find their origin in the prediction of the flow at high liquid fraction which is very sensitive to the discretization scheme. One conclusion of this study is that it seems to be unrealistic to search a reference solution when channels form during solidifcation. One common point is that channels are predicted by all contributors, which mean that at minimum the results can indicate a sensitivity to channel formation. At the reverse, concerning the macrosegregation pattern the solution is similar for all the contributions. The reason is that the macrosegregation continues to evolve until low liquid fraction (typically until the liquid fraction is greater than 0.3). The calculation of the flow in the region of low liquid fraction is less sensitive to the discretization of the convective terms because these terms become negligible. Similar conclusions have been drawn for the second solidification case investigated in this benchmark exercise for a Sn-10wt%Pb alloy [26].

This benchmark exercise is now continued by a comparison of thermal and solutal natural cases without solidification in order to check the accuracy of the codes. Moreover, a case without channels formation has been defined [23]. Two codes have been used, one based on a finite volume method with a second order scheme to discretize the convective terms and the second one based on a meshless method. Even if a unique converged solution has not been found at the moment, it seems possible by refining the mesh to get a reference solution.

References

[1] C. Beckermann, Modelling of Macrosegregation: Applications and Future Needs, *Int. Mater. Rev.*, 2002, vol. 47, 243-261.

[2] S. Ganesan and D.R. Poirier, Conservation of mass and momentum for the flow of interdendritic liquid during solidification, *Metall. Trans.*, 1990, vol. 21B, 173-181.

[3] D. R. Poirier, P. J. Nandapurkar, and S. Ganesan, The energy and solute conservation equations for dendritic solidification, *Metall. Trans.*, 1991, vol. 22B, 889-900.

[4] J. Ni and C. Beckermann, A Volume-Averaged Two-Phase Model for Solidification Transport Phenomena, *Metall. Trans.*, 1991, vol. 22B, 349-361.

[5] W. D. Bennon and F. P. Incropera, A continuum model for momentum, heat and species transport in binary solid-liquid phase change systems. 1. Model formulation, *Int. J. Heat Mass Transfer*, 1987, vol. 30, 2161-2170.

[6] H. Combeau, J.-M. Drezet, A. Mo and M. Rappaz, Modeling of microsegregation in macrosegregation computations, *Metall. Trans.*, 1996, vol. 27A, 2314-2327.

[7] C. Y. Wang and C. Beckermann, A Unified Solute Diffusion Model for Columnar and Equiaxed Dendritic Alloy Solidification, *Mater. Sci. Eng*., 1993, vol. 171, 199-211.
[8] M. C. Schneider and C. Beckermann, Formation of Macrosegregation by Multicomponent Thermosolutal Convection during Solidification of Steel, *Metall. Trans.*, 1995, vol. 26A, 2373-2388.
[9] M.C. Schneider, J. P. Gu, C. Beckermann, W. J. Boettinger and U. R. Kattner, Modeling of Micro- and Macrosegregation and Freckle Formation in Single-Crystal Nickel-Base Superalloy Directional Solidification, *Metall. Trans. A*, 1997, vol. 28A, 1517-1531.
[10] J. P. Gu and C. Beckermann, Simulation of Convection and Macrosegregation in a Large Steel Ingot, *Metall. Trans. A*, 1999, vol. 30A, 1357-1366.
[11] M. Wu, A. Fjeld and A. Ludwig, Modelling mixed columnar-equiaxed solidification with melt convection and grain sedimentation - Part I: Model description , *Comp. Mat. Sc*., vol. 50, 1, 2010, 32-42.
[12] J. Li, M. Wu, J. Hao and A. Ludwig, Simulation of channel segregation using a two-phase columnar solidification model – Part 1: Model description and verification, *Comp. Mat. Sc*., vol. 55, 2012, 407-418.
[13] L. Thuinet, H. Combeau, A New Model of Microsegregation for Macrosegregation Computation in Multicomponent Steels. Part I: Theoretical Formulation and Algorithm, *Comp. Mat. Sc*., 45 (2), 2009, 294-304.
[14] A. Kumar, B. Dussoubs, M. Založnik, H. Combeau, Effect of discretization of permeability term and mesh size on macro- and meso-segregation predictions, *Journal of Physics D:Applied Physics*, vol. 42, Issue 10, 2009, 105503-105515.
[15] H. Combeau, M. Založ nik, S. Hans, and P. E. Richy, Prediction of macrosegregation in steel ingots: influence of the motion and the morphology of equiaxed grains, *Metall. Trans.*, vol. 40B, June 2009, 289-304.
[16] T. Sawada, K. Oikawa, K. Anzai, Simplified three-dimensional macro segregation model and its application to directional solidification of Sn-Bi alloys, *MCWASP XII*, TMS, Warrendale, PA, USA, 2009, 303-310.
[17] K. Nakajima, H. Zhang, K. Oikawa, M. Ohno and Pär G. Jönsson, Methodological progress for computer simulation of solidification and casting, *ISIJ*, vol. 50, N°12, 1274-1234.
[18] M. Bellet and col., Call for contributions to a numerical benchmark problem for 2D columnar solidification of binary alloys, *International Journal of Thermal Sciences*, 48 (11), 2013-2016.
[19] Thétis, 2009, code de mécanique de fluides, http://thetis.enscbp.fr/
[20] N. Ahmad, H. Combeau, J.-L. Desbiolles, T. Jalanti, G. Lesoult, J. Rappaz, M. Rappaz and C. Stomp, Numerical simulation of macrosegregation: a comparison between finite volume method and finite element method predictions and a confrontation with experiments, *Metall. Trans.*, 29A, 1998, 617-630.
[21] W. Liu, C. Xie, M. Bellet, H. Combeau, 2-Dimensional FEM modeling of macrosegregation in the directional solidification with mesh adaptation, *Acta Metall. Sin.*, 22 (2009) 233-240.
[22] Voller V.R., Brent A. and Prakash C. (1989), The Modeling of Heat, Mass and Solute Transport in Solidification Systems, *Int. J. Heat Mass Transfer*, Vol. 32, 1719-1731.
[23] G. Kosec, M. Založnik, B. Šarler and H. Combeau, A meshless approach towards solution of macrosegregation phenomena, *Computers, Materials and Continua*, Vol. 22, Issue 2, 2011, 169-195.
[24] Hachani L, Saadi B, Wang X D, Nouri A, Zaidat K, Belgacem Bouzida A, Ayouni-Derouiche L, Raimondi G and Fautrelle Y 2011, *Int. J. Heat and Mass Transfer,* vol. 55, 2012, 1986-1996.
[25] http://www.ijl.nancy-universite.fr/benchmark-solidification
[26] H. Combeau and col., A numerical benchmark on the prediction of macrosegregation in binary alloys, *TMS Annual Meeting*, vol. 2, 2011, 755-762.
[27] J. H. Ferziger, M. Peric, Computational Methods for Fluid Dynamics, Springer, 1997, ISBN 3-540-59434-5.

[28] V. F. De Felice, K. O. Tveito, M. Založnik, H. Combeau, M. M'Hamdi, Three-dimensional study of macro- and mesosegregation formation in a rectangular cavity cooled from one vertical side, *Modeling of Casting, Welding and Advanced Solidification Processes XIII, June 17–22, 2012, Schladming, Austria, in press (2012).*

Acknoledgments

This work was funded by the French National Research Agency (ANR) in the framework of the 'Programme Blanc', as part of the project SMACS (ANR-07-BLAN-190).

Nomenclature

$\langle h \rangle$	average enthalpy per unit mass, $J.\ kg^{-1}$	m_l	liquidus slope (K wt. pct.$^{-1}$)
T	temperature, K	k_0	partition coefficient
C_p	specific heat per unit mass, $J.kg^{-1}.K^{-1}$	*Greek symboles*	
V	average velocity of the liquid, $m.s^{-1}$	β_T	thermal expansion coefficient, K^{-1}
k	thermal conductivity, $W.m^{-1}.K^{-1}$	β_c	solutal expansion coefficient, $(wt.\ pct.)^{-1}$
g_α	volume fraction of the phase α= l or s	μ	dynamic viscosity, $Pa.s$
$\boldsymbol{g}$	gravity acceleration, $m.s^{-2}$	ρ	density, $kg.\ m^{-3}$
K	permeability, m^2	*Subscripts and superscripts*	
p	pressure (Pa)	l	liquid phase
$\langle C \rangle$	average mass solute fraction	s	solid phase
C_l	average mass solute fraction in the liquid phase		